Velocity fluctuations in dense granular flows

John J. Drozd and Colin Denniston
Department of Applied Mathematics, The University of Western Ontario, London, Ontario, Canada N6A 5B8
(Received 16 May 2008; published 10 October 2008)

We use simulations to investigate velocity fluctuations in dry granular flow. Our system is comprised of mono- and polydisperse sets of spherical grains falling down a vertical chute under the influence of gravity. We find three different classes of velocity distributions depending on factors such as the local density. The class of the velocity distribution depends on whether the grains are in a free-fall, fluid, or glassy state. The analytic form of the distributions match those that have been found by other authors in fairly diverse systems. Here, we have all three present in a single system in steady state. Power-law tails that match recent experiments are also found but in a transition area suggesting they may be an artifact of crossover from one class of velocity distribution to another. We find evidence that the transition from one class to another may correspond to a second order dynamical phase transition in the limit that the vertical flow speed goes to zero.

DOI: 10.1103/PhysRevE.78.041304 PACS number(s): 45.70.Mg, 83.80.Fg, 05.20.Dd

I. INTRODUCTION

Dissipative granular fluids are difficult to characterize because they are not typically in any sort of equilibrium state. Unlike a closed system of elastic particles, an initially homogeneous steady-state dissipative granular fluid typically develops nonuniform, and even singular, spatial variations in density, momentum density, and temperature [1,2]. Even static granular systems are typically the result of such a rapid quench in temperature that they are in glasslike states and hence not easily described by equilibrium thermodynamics [3]. It is, however, possible to produce a fairly homogeneous steady-state system if there is a steady energy input to compensate for the energy lost in collisions. This can be achieved by vibrating the system (or a wall), shearing the system, allowing grains to fall in a chute, or adding stochastic noise (in a simulation).

Theoretical and computational studies of steady state suggest that these inelastic systems can be subdivided into phases with different velocity distributions [4–8]. For instance, Esipov and Poschel [4] suggested the existence of a granular gas, a condensed phase, and a collapsing condensed phase. They arrived at these phases by studying analytically the kinetic energy distribution function satisfying the Boltzmann equation. They also studied this function numerically for a system composed of a circular wall maintained at a constant temperature, enclosing inelastic hard disks with binary collisions and found that their analytical formulation suited the simple cases of steady-state flows. Noije and Ernst [5] solved the nonlinear Enskog-Boltzmann equation for a freely evolving and a heated system of hard disks or spheres and found that their freely evolving system coincided with the result of Esipov and Poschel. Ernst and Brito [6,7] analyzed the nonlinear Boltzmann equation by adding a stochastic noise or stochastic force to the microscopic equations of motion. They considered three types of thermostats, namely, a Gaussian thermostat, a white noise thermostat, and a gravity thermostat and found that the form of the high-energy tails in the velocity distributions, whether it be Gaussian, stretched exponential, or power-law depends on the type of thermostat and on the type of interaction model. Ben-Naim and Machta [8] performed theoretical derivations and numerical simulations of inelastic gases to study stationary velocity distributions that obey the Boltzmann equation and found that their velocity distributions have a high-energy tail corresponding to a range from high to low velocities, and that steady states can be realized by injecting energy at high velocities. They randomly raised particles to high velocities such that energy was injected only at the tail of the distribution. This did not change the collision dynamics but rather set a scale for the most energetic particles. While these studies have given insight into granular dynamics, experiments rarely have an analog of stochastic noise or direct injection at one end of the spectrum or other easily controlled energy input.

There have been many experiments used to measure velocity distributions. Several experiments have studied granular flow in a vertical channel [9–11]. Savage [12] used fiber-optic probes to measure velocity profiles in a vertical channel at the sidewalls. Natarajan, Hunt, and Taylor [9] found that their velocity measurements showed that the vertical flows had a central uniform flow region and a shear flow region close to the vertical sidewalls. They also found that the magnitude of the fluctuating velocities in the transverse direction increased from the center towards the sidewalls. Menon and Durian [13] used diffusing-wave spectroscopy to measure fluctuation velocities of glass beads in a vertical chute and found a power-law relationship between mean fluctuation velocities and flow velocity. Losert, Cooper, Delour, Kudrolli, and Gollub [14] used a vibrated granular experiment in which they measured velocity statistics for a layer of inelastic colliding beads driven by a vertically oscillating boundary. They found when external excitation was high enough to generate accelerations 3–8 times that of gravity, the probability distribution of the horizontal velocity $P(v) \sim \exp(-|v/v_c|^{1.5})$. For cooler particles in the absence of excitation, they found an exponential velocity distribution. Rouyer and Menon [15] similarly used vertical vibration of a vertical plane to measure velocity fluctuations to arrive at $P(v) \sim C \exp[-\beta(|v|/\sigma)^{\alpha}]$ with $\alpha = 1.55 \pm 0.1$ at all the frequencies and amplitudes that they used. Recently, Moka and Nott [16] used video imaging and particle tracking to measure particle velocity distributions in slowly flowing granular

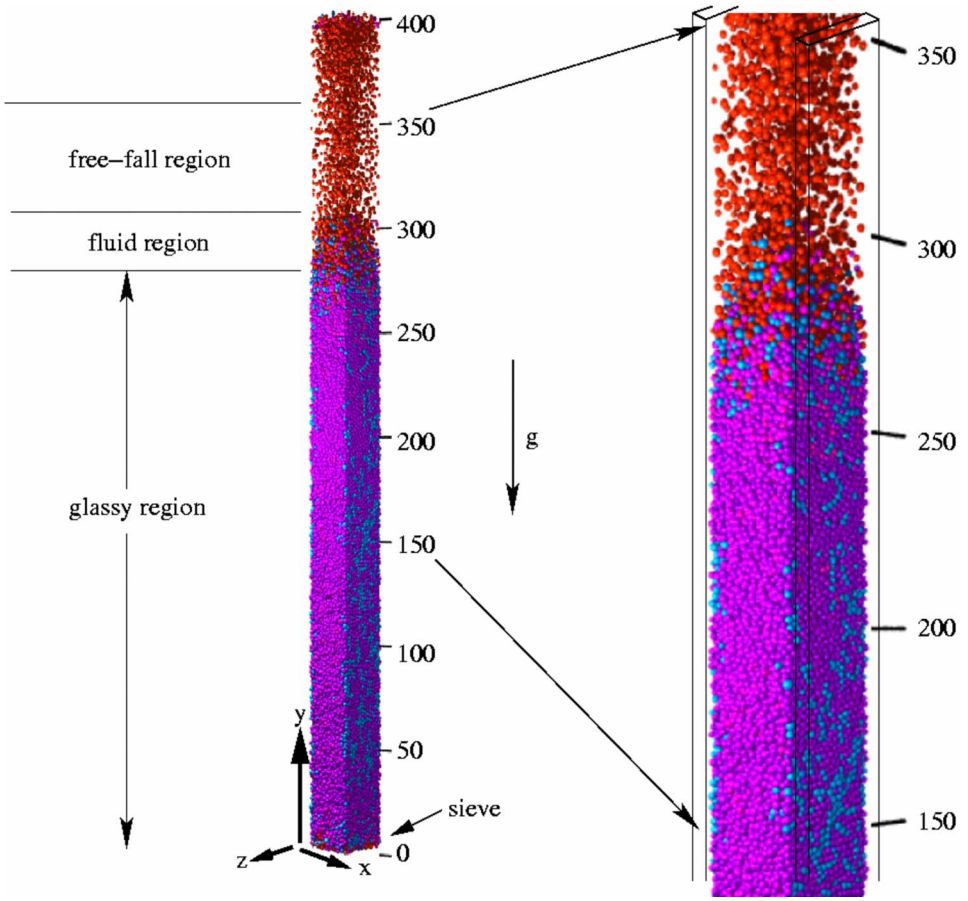

FIG. 1. (Color online) Section of a simulation involving 43 200 grains with 15% polydispersity. The system size is $32a \times 32a \times 400a$. There are reflective walls at $x=0$ and $x=L_x$, periodic boundary conditions in the z direction, and a finite probability of reflection at the bottom of the chute (at $y=0$).

material down a vertical channel. They found an abrupt change in the mean velocity in shear layers near the sidewalls, but that it was constant in the middle region. However, in contrast to [9,17,18], they found velocity fluctuations to be larger in the center of the channel than at the sidewalls. They found the velocity distribution to be non-Gaussian and anisotropic, following a power law at larger velocities and that this distribution was identical in the outside shear layer and in the middle core. We will compare our simulation results with many of these experiments throughout this paper. As we shall show, the velocity distributions measured in these experiments are very different in different regions and a consistent interpretation of experiment therefore requires knowing what phase is being studied. One of the advantages of the system we are studying is that, as we will demonstrate below, we can see all of these phases in a steady-state configuration that can be easily realized experimentally.

In this paper we will look at velocity distributions in the gravity-driven flow shown in Fig. 1. The simulation is set up to mimic experiments of chute flow [9,12,13,16]. Spherical grains are dropped in from the top of a rectangular chute and fall under the influence of gravity. There are flat walls at the left and right (x direction) of the chute and periodic boundary conditions at the front and back (z direction). At the bottom of the chute ($y=0$), there is a sieve which controls the flow rate. When a particle leaves the bottom a new particle is placed at the top to maintain a constant number of particles in the system. We studied a similar system in a recent letter [19] and in two dimensions (2D) in an earlier work [21]. Based on the distributions of times between collisions, we found our simulation had three regions or phases, which we labeled and justified as a glassy region, a fluid region, and a free-fall region. We found there was a different collision time distribution for each of these three distinct phases [19]. Now, in our present study we also find these three phases can be characterized by the form of their respective velocity distributions.

In the first section we describe the simulations and the steady-state configuration of the mean velocity and velocity fluctuations. We then examine the distribution of velocity fluctuations in detail. Different velocity distributions are found depending on whether the system displays characteristics of a fluid or a glass. The apparently conflicting results seen in experiments [9,16] are found to be related to different phases in our simulations. We then examine the relation of the velocity fluctuations to the distribution of times between collisions. We find evidence that the transition from one class to another may correspond to a second-order dynamical phase transition in the limit that the vertical flow speed goes to zero.

II. MODEL

A typical snapshot from one of our simulations is shown in Fig. 1. As indicated in Fig. 1, there are three regions, which we label as a glassy region, a fluid region, and a free-fall region. These labels will be referenced throughout this paper and were justified in our previous study [19]. Spherical

grains are dropped in from the top of a rectangular chute in the free-fall region and the grains accelerate at 1 g where g is the acceleration due to gravity (units are given in footnote [20]). There are flat walls at the left and right (x direction) of the chute and periodic boundary conditions at the front and back (z direction). This geometry is similar to that studied experimentally in [16] where similarly rough sidewalls were used. Periodic boundary conditions in z reduce wall effects and allow us a translationally invariant direction to average data over. In experiments a similar situation is obtained by having a system much longer in z than x. At the bottom of the chute ($y=0$), grains are reflected with a probability p (typically $p=90\%$) which models a sieve at the bottom of the chute. This has the same effect as a mesh that was used in the chute experiment described by Menon and Durian [13]. By using a sieve to restrict our flow of particles, we are able to also model other experiments that use a restricting outlet as in the experiment by Moka and Nott [16]. As detailed later, we were able to reproduce the results of both of these experiments. We maintain a constant number of particles in our simulation by having new particles placed at the top of the chute when an old particle leaves the bottom. We ran simulations with different initial conditions for grains at the top of the chute, for instance, we started particles at rest at the top of the chute and let them fall under the influence of gravity, gave them random velocities equal to the grains leaving the system at the bottom, and found no change in our results that are reported in this paper or in our previous paper [19].

The velocities of two grains after collision $\dot{\mathbf{r}}_1'$ and $\dot{\mathbf{r}}_2'$ in terms of the velocities before collision, $\dot{\mathbf{r}}_1$ and $\dot{\mathbf{r}}_2$, are

$$\begin{pmatrix} \dot{\mathbf{r}}_1' \\ \dot{\mathbf{r}}_2' \end{pmatrix} = \begin{pmatrix} \dot{\mathbf{r}}_1 \\ \dot{\mathbf{r}}_2 \end{pmatrix} + \frac{(1+\mu)}{(m_1+m_2)} \begin{pmatrix} -m_2 & m_2 \\ m_1 & -m_1 \end{pmatrix} \begin{pmatrix} \dot{\mathbf{r}}_1 \cdot \mathbf{q} \\ \dot{\mathbf{r}}_2 \cdot \mathbf{q} \end{pmatrix} \mathbf{q}, \quad (1)$$

where $\mathbf{q}=(\mathbf{r}_2-\mathbf{r}_1)/|\mathbf{r}_2-\mathbf{r}_1|$, and μ is the coefficient of restitution. Such collision models of granular flow have a long history [22,23]. μ is a velocity-dependent restitution coefficient described by the phenomenological relation [24–26],

$$\mu(v_n) = \begin{cases} 1-(1-\mu_0)(v_n/v_0)^{0.7}, & v_n \leqslant v_0 \\ \mu_0, & v_n \geqslant v_0. \end{cases} \quad (2)$$

Here v_n is the component of relative velocity along the line joining the grain centers, μ_0 is the asymptotic coefficient at large velocities, and $v_0=\sqrt{2ga}$ [27]. Equation (2) effectively makes the ball collisions become more elastic as the collisions become weaker as seen in experiments [24–26].

Experiments clearly show that the weight of a dense column of grains is supported by the walls [28,29]. This is also desirable in a simulation as it will lead to a pressure independent of height in the dense glassy region. Specular reflection will *not* accomplish this. In experiments, spin and tangential friction would result in a loss of vertical momentum at rough-surfaced walls. While we do not have spin and friction in our simulation, we need a vertical loss to model the experiment. We achieved this by modeling the left and right walls as rough walls by having particles reflect off the left and right walls of the chute with a partial loss, typically 10% in their vertical (y) velocity. The precise value of the partial loss made little qualitative difference. Rough walls enabled our flowing grains to see a wall support and a shearing regime similar to that found in experiments [9,16].

A parameter that turns out to be surprisingly important is the polydispersity of the grain sizes. Here, we use a Gaussian distribution of grain radii and a polydispersity of 15% means that the standard deviation of the particle radii is 0.15 if the mean radius is 1. Typically even experiments that use "monodisperse" grains have some small polydispersity on an order of a few percent. We have performed simulations at a range of polydispersity from 0 to 15% and find even a few percent can give significantly different results from pure monodisperse systems. This is because the geometry in the packing of particles of different sizes dictates whether particles crystallize (in the monodisperse case) or go into a glassy state (in the polydisperse case). This has a significant impact on collision time power laws [19].

III. STEADY-STATE CONFIGURATION

We started a configuration with particles racked in a three-dimensional (3D) rectangular array with a Gaussian distribution of randomized initial velocities with standard deviation 0.8. From this initial configuration, we ran our simulation and we plotted the number of collisions over time. When the total number of collisions per unit time remained level over time, our simulation had reached a steady state. For our 3D system, steady state was achieved after about 100 time units, enough time for all grains to move through the system once.

The number of grains was chosen so that there would be a large free-fall region at the top (so the results would not depend on specifics of the injection at the top) but enough so that there would also be a large glassy region (50%–65% of the system). Flow velocity is controlled by the reflection probability p at the sieve. However, the qualitative behavior and division into three phases is not that dependent on the flow velocity until the sieve restriction is nearly removed (near $p \leqslant 0.10$).

Typical steady-state configurations of the local density, measured as volume fraction, and vertical (y) velocity down the center of the chute are shown in Fig. 2 as a function of y (height). A clear difference in the density profile of a nearly monodisperse (1%) [dashed line in Fig. 2(a)] and the system with 15% polydispersity (solid line) is clearly visible. In the more polydisperse system the density in the region we have labeled as fluid steadily increases until it hits 0.60 volume fraction and is then constant in the main bulk of the column. However, the nearly monodisperse system shows a steady, nearly linear, increase in density from a volume fraction of 0.64 to nearly 0.70 near the bottom of the channel. This indicates that the nearly monodisperse system continues to order (i.e., crystallize) as it travels down the channel, even in the very dense region.

As previously indicated there are three regions, which we label as a glassy region, a fluid region, and a free-fall region. These labels were justified in our previous work [19]. In the free-fall region the grains accelerate at 1 g and collisions are rare enough that the acceleration is unimpeded as shown in Fig. 2(c). In the liquid region the density is sufficiently high that collisions mix the grains, but the distribution of collision

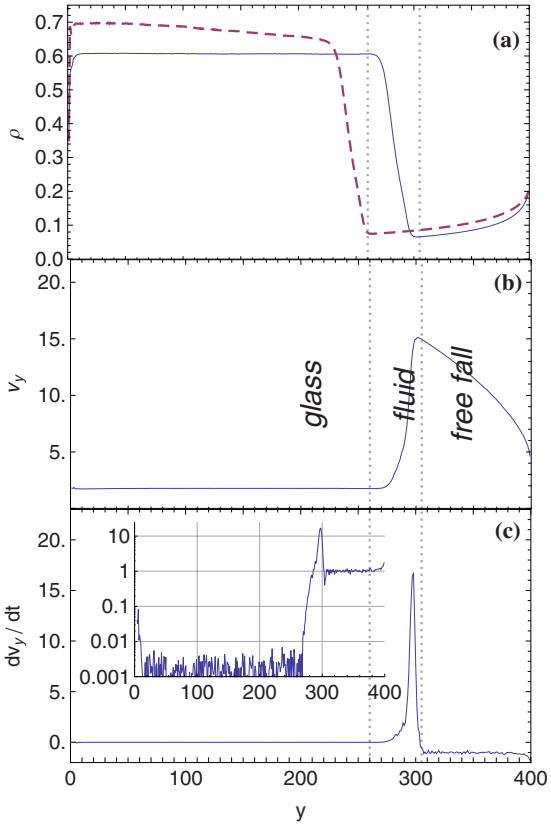

FIG. 2. (Color online) Average (a) density (volume fraction) for 1% (dashed line) and 15% polydispersity (solid line) along the height of a 3D chute. For 15% polydispersity, (b) the y velocity and (c) the average acceleration as measured by the material derivative. The inset in (c) shows the same data on a logarithmic scale, clearly indicating the acceleration of 1 g down in the free-fall region. This justifies the "free-fall" label. Note that this plot takes an absolute value so the acceleration is actually −1 g and changes sign at a height of 300. This is for a 3D $32a \times 32a \times 400a$ 15% polydisperse simulation with an asymptotic coefficient of restitution $\mu_0 = 0.9$.

times (the time between collisions for a given grain) is exponential, meaning that collisions are largely independent. In the glass region, the collision time distribution is a power law and thus there are collisions at a wide range of time scales [19]. We should emphasize, as shown in [19], that monodisperse systems continue to crystallize so they are not truly a glass.

The velocity profile in a cross section of the flow is also very different in the fluid and glass regions. As can be seen in Figs. 3(a) and 3(b), in the fluid region the fluid velocity fits a parabolic flow as expected for a fluid with a constant viscosity in a pressure gradient (Poiseuille flow) [30]. In the glassy region, jamming or plasticity occurs giving way to a plug type profile in the 15% polydisperse case. More pronounced kinks occur in the 1% polydisperse (essentially monodisperse) case as shown by the ⋆'s in Fig. 3(a). These kinks are associated with fracture along crystal domain walls. Similar profiles are seen in two-dimensional flow where it is easy to see the crystallization and domain walls (see Fig. 4). This crystallization is not seen initially in the monodisperse systems, but once it develops it persists for as

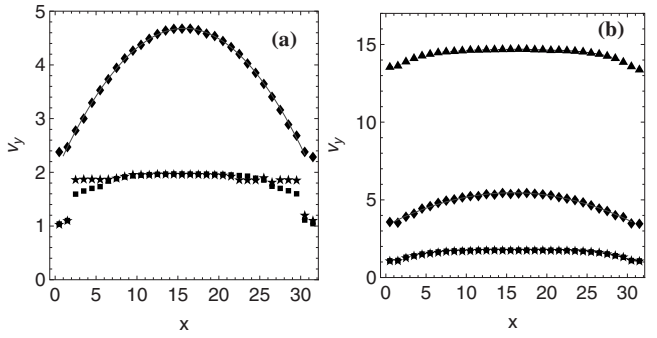

FIG. 3. Vertical velocity profiles along a width of 3D chute in 32 by 32 systems at different heights. (a) is for 1% polydisperse systems with ♦ in the fluid phase at $y = 250$ (averaged over 500 time units), ■ in the disordered solid phase at $y = 200$, and ⋆ in the crystallized phase at $y = 150$ (averaged over five time units). (b) is for a 15% polydisperse system at different heights with the ▲ in the transition region of the free-fall to fluid phase at $y = 310$ (this plug profile was similar in the transition region of the free-fall to fluid phase for the 1% polydisperse system), ♦ in the fluid phase at $y = 290$, and the others in the glassy phase. The lines in the fluid phase are fits to a parabola. The discontinuities in (a) indicate fracture and while these discontinuities move around somewhat over time, the average profile does not become smooth.

long as our longest simulations. This suggests that once a seed crystal forms, it acts as a template for the material coming out of the liquid phase. This, and our previous work that showed different exponents for poly- and monodisperse sys-

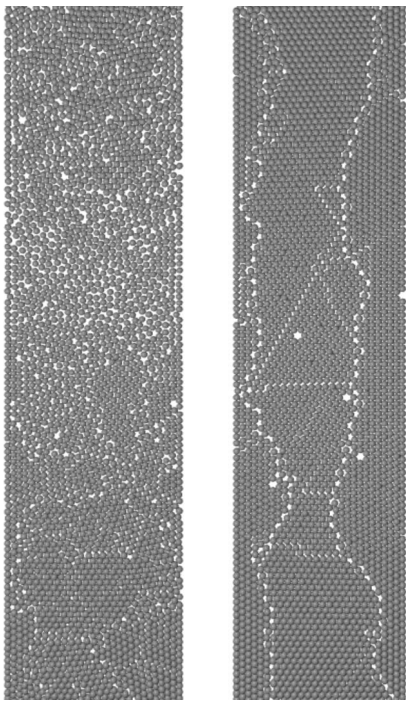

FIG. 4. Visualization of 2D sphere simulation showing (a) random packing in monodisperse spherical grains at the early stages of the simulation (at a time of 200 in simulation units), and (b) crystallization in monodisperse spherical grains at the later stages of the simulation (at a time of 3200).

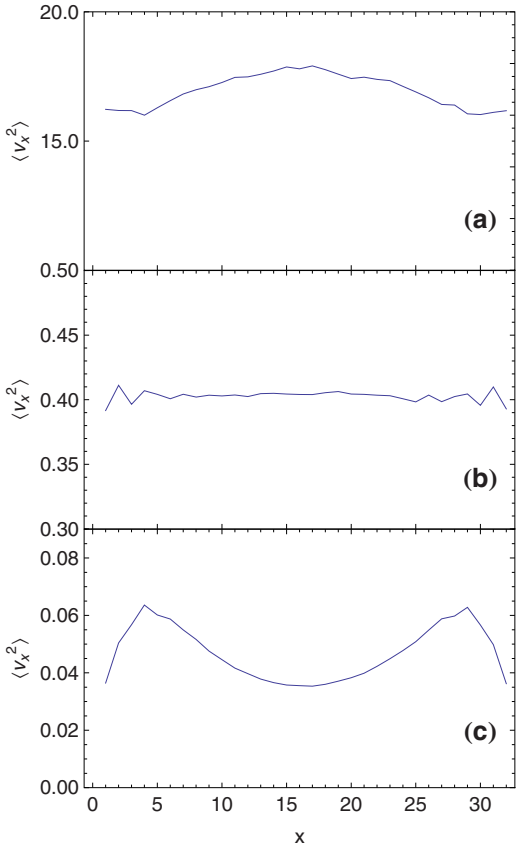

FIG. 5. (Color online) Plot of $\langle v_x^2 \rangle$ versus the width x in the (a) fluid, (b) glass-fluid transition, and (c) glassy regions for 15% polydisperse 3D simulation. The curves represent data with an asymptotic coefficient of restitution of μ_0 of 0.97. Data is averaged over 10 ball diameters in height.

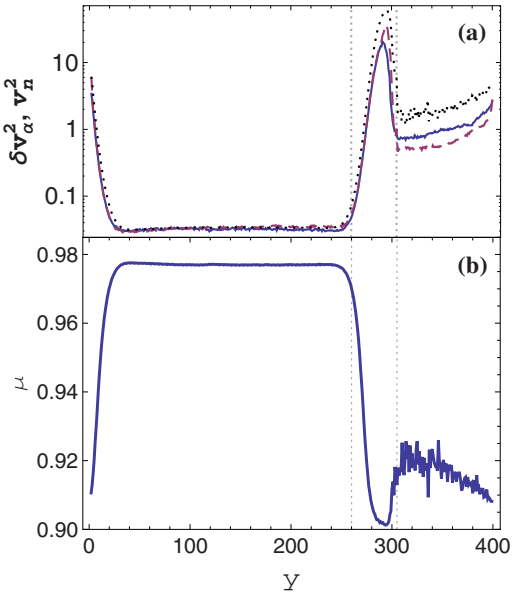

FIG. 6. (Color online) Plot of (a) δv_x^2 (solid line), δv_y^2 (dashed line), and the square of the mean relative velocity in normal direction during a collision v_n^2 (dotted line) versus the height for 15% polydisperse 3D simulation with an asymptotic coefficient of restitution μ_0=0.9 and (b) the velocity-dependent coefficient of restitution $\mu(v_n)$. Note that plot (a) is a semilogarithmic plot.

tems for the power-law distribution of collision times [19], suggests that the dynamics of the very dense monodisperse and polydisperse systems are significantly different. The dynamics of the dense polydisperse systems are more akin to regular structural glasses, whereas the dense monodisperse systems are more similar to fracture dynamics in crystalline systems.

The flow profile in the free-fall region depends somewhat on the profile that the grains start with at the top. If the grains start with a uniform distribution of velocities at the top, independent of their x position, then the profile will start out flat. As the grains fall down the channel they are slowed at the wall and the fluidlike phase gradually grows in from the walls. This gives what looks like a pluglike profile as the fluid phase is approached. However, the plug profile here is due to very different reasons than those causing the plug profile in the glassy region. In the glassy region the central portion of the flow is jammed into a true plug, whereas in the free-fall region the plug flow is from the retention of the input profile at the top of the column as shown by the top profile (▲'s) in Fig. 3(b).

The characteristics of the velocity fluctuations ($\delta v_\alpha^2 \equiv \langle (v_\alpha - \langle v_\alpha \rangle)^2 \rangle$) are also different in the different regions. Figure 5 shows the profile of the velocity fluctuations in the different regions. In the fluid region (and the free-fall region which is similar) the grains gain enough kinetic energy between collisions (from acceleration due to gravity) to more than compensate for the loss in kinetic energy in collisions. As a result, the system is hotter ($\delta \mathbf{v}^2$ is bigger) in the middle and heat flows *out* from the center towards the walls (we define the granular temperature as $T \equiv [\langle v_x^2 \rangle + \langle (v_y - \langle v_y \rangle)^2 + \langle v_z^2 \rangle]/2$ and heat flow is proportional to ∇T). In the glass phase, the system is colder ($\delta \mathbf{v}^2$ is smaller) in the middle and heat flows *in* from the shear zones near the walls. Figure 6 shows that $\partial_y T > 0$ in the liquid and free-fall regions, so we expect heat should flow down the channel there, but that there should be no vertical heat flow in the glass (as $\partial_y T = 0$ in the glass). As Fig. 6(a) shows, the square of the typical normal velocity v_n^2 encountered in a collision essentially tracks the velocity fluctuations. In the fluid and free-fall regions the typical v_n is sufficiently high that $\langle \mu \rangle$ is close to its asymptotic value μ_0. In the glassy region v_n is typically much smaller and $\langle \mu(v_n) \rangle$ is closer to 1.

Elastic hard spheres undergo a fluid-solid phase transition [31]. Inelastic granular systems have a similar transition [32–35]. Theory suggests that in inelastic systems these phases can be further subdivided into dynamical phases with different characteristic velocity distributions [4–8]. The different phases we see in our simulations are closely aligned with the phases suggested by Esipov and Poschel [4], as we shall show in more detail below. Experiments, however, often have not clearly identified which phase is being observed. This has led to what at first appears to be potentially conflicting results. Moka and Nott [16] observe a phase that exhibits pluglike flow and is hotter in the interior of the system. This corresponds to the free-fall to fluid transition region in our system. As in the experiment, our velocity in this transition region (▲'s) of Fig. 3(b), also shows a plug

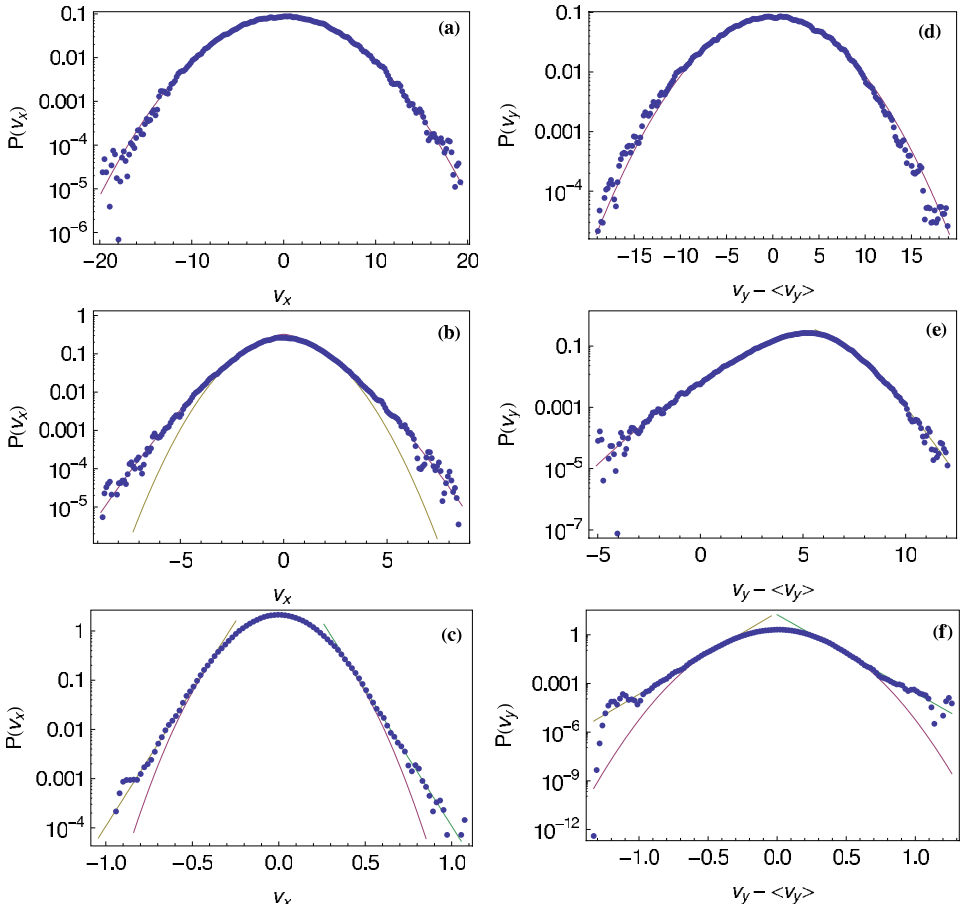

FIG. 7. (Color online) x-velocity distributions in (a) free-fall, (b) fluid, and (c) glassy region and y-velocity distributions in (d) free-fall, (e) fluid, and (f) glassy region for a 15% polydisperse simulation. Note that $\langle v_x \rangle = 0$, so we plotted the x-velocity distribution as $|v_x| = |v_x - \langle v_x \rangle|$, whereas $\langle v_y \rangle \neq 0$, so we plotted the y-velocity distribution as $|v_y - \langle v_y \rangle|$. These velocity distributions were taken at heights in the chute at $h = 300$ in the free-fall region, $h = 270$ in the fluid region, and $h = 190$ in the glassy region. Fits are shown with the solid line ($\mu_0 = 0.97$).

profile. This is because the particles at the top of the chute are given random velocities, and thus have, on average, a flat velocity profile at the top. As the particles travel down to the free-fall to fluid transition region this develops into a plug profile as the fluid region grows in at the walls. The corresponding plot of granular temperature shown in Fig. 5(a) is hotter in the middle as collisions with the walls are slowing the grains in this region more than in the interior where there are few collisions. More typically, experiments [9,17,18] see the interior being colder corresponding to our glassy phase. Clearly, the system supports a finite shear stress in the central glassy region with continuous, plastic deformation along the boundary. This is shown in the plug flow profile in the glassy region of our simulation, ($\star$'s) of Fig. 3(b), and in the corresponding plot of granular temperature in Fig. 5(c), which shows the temperature to be colder in the middle. As we shall show below, the velocity distributions are very different in these three different regions and a consistent interpretation of experiment therefore requires knowing what phase is being studied. Few experiments tend to pin this down and the implicit assumption appears to be that the entire system is in one phase, something that is clearly not the case. We hope that future experiments will pay more attention to measuring properties such as density and flow rate as a function of height to clearly identify the phases present. One of the advantages of the system we are studying is that we can see all of these phases in a steady-state configuration that can be easily realized and thus studied experimentally.

IV. VELOCITY DISTRIBUTIONS

A normal fluid in local equilibrium in the canonical ensemble has velocity fluctuations $\delta\mathbf{v}$ distributed about the local mean velocity $\mathbf{v}$ in a Gaussian,

$$P(\delta\mathbf{v}) \sim \exp\left(-\frac{\delta\mathbf{v}^2}{k_B T}\right). \tag{3}$$

Numerous experiments and simulations [5,8,14–16,36] have shown that velocity fluctuations in granular materials do not generally follow such a distribution. This is not that surprising as energy is constantly being lost (due to the inelastic collisions) and the assumption of local equilibrium is dubious in most of the system. However, there is also conversion of potential energy to kinetic energy due to the grains falling so the possibility of kinetic energy loss from collisions balancing kinetic energy gain can occur, at least in some regions. In fact we find two regions in the system where the distribution of v_x *is* Gaussian.

The first location is in the free-fall region. Grains are placed at the top of the chute at a random x and z position and with a small random velocity ($\langle v_\alpha^2 \rangle$ similar to at the bottom of the chute but from a uniform distribution). Even though the starting velocity distribution is not Gaussian, the velocity distribution at the top becomes Gaussian within 5 ball radii of the top (we measured the distribution every $5a$ from top to bottom). This is not surprising if one recalls the central limit theorem (particles start at top with velocities

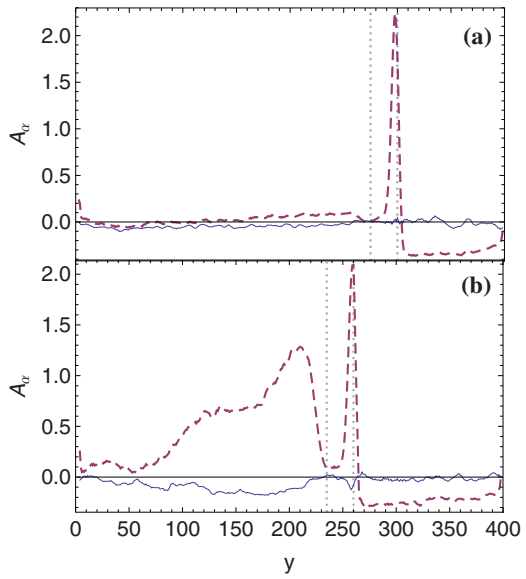

FIG. 8. (Color online) $A_\alpha=(\delta v_\alpha^2-\delta v_x^2)/\delta v_x^2$, the anisotropy in the velocity fluctuations relative to the x direction. A_y (dashed line) and A_z (solid line) are shown for the 3D (a) 15% polydisperse system and (b) 1% polydisperse (essentially monodisperse) system with an asymptotic coefficient of restitution $\mu_0=0.9$. The vertical dashed lines indicate the fluid transition region.

independent of nearby particles). The v_x distribution remains Gaussian in the free-fall region [see Fig. 7(a)], but narrows as the grains fall (i.e., the standard deviation $\langle v_x^2\rangle^{1/2}$ becomes smaller as shown in Fig. 6). The distribution narrows as a result of collisions dissipating kinetic energy. This energy could, in principle, be recouped from gains from the conversion of potential energy to kinetic energy, and as we will see below this does affect the v_y distribution. However, the v_x fluctuations are largely decoupled from the v_y fluctuations in the free-fall region. This can be seen in the anisotropy of the velocity fluctuations shown in Fig. 8 for $\mu_0=0.9$. There is a significant difference in the anisotropy in the polydisperse versus monodisperse (1% polydisperse) cases when we compare Fig. 8(a) versus Fig. 8(b). The reason we find this difference in anisotropy in the glassy phase is that in the monodisperse case, the particles become more ordered and tend to crystallize causing forces to translate along straight line chains of particles. Thus the monodisperse particles become more correlated. In the polydisperse case the particles are more disordered and thus less correlated. We reported this finding in our previous paper [19]. In the remainder of the paper we will focus on the 15% polydisperse systems. Also, in the free-fall region, δv_x^2 and δv_z^2 differ significantly from δv_y^2. In the transition from free fall to fluid, this anisotropy abruptly changes sign and then drops close to zero in the liquid phase. We will discuss this transition region more below after we have discussed the distributions in the main phases.

In the fluid phase, the v_x distribution fits a Gaussian at low v_x but has stretched exponential tails as shown in Fig. 7(b). These tails gradually fill in the whole distribution to the point where the entire distribution can be well fit to a function $A\exp(-(|v_x/v_0|^\alpha)$, with $\alpha=3/2$, as shown in Fig. 7(b).

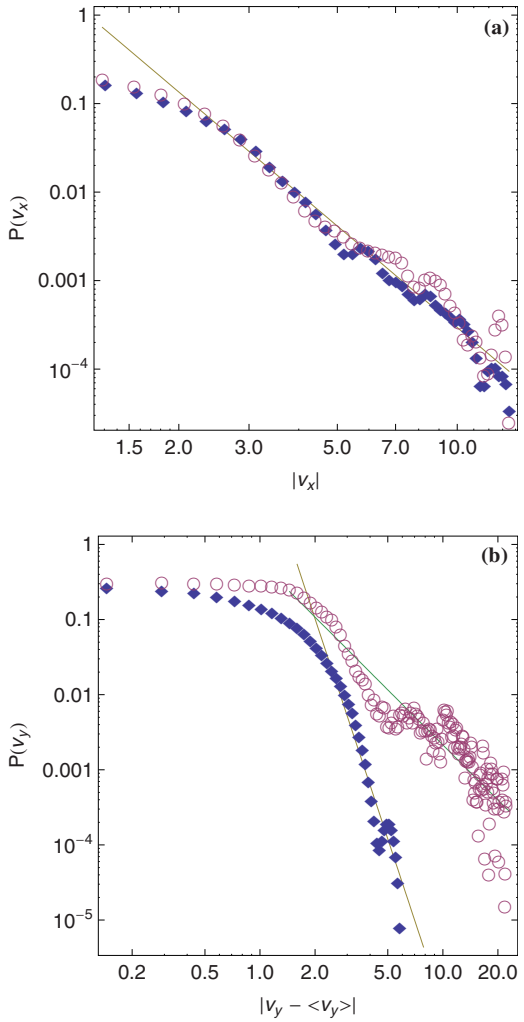

FIG. 9. (Color online) (a) Log-log plots of x-velocity distributions in a transition region between free fall and fluid. The line is a power-law fit $P\sim 1/v^\beta$ with $\beta=3.8$. (b) y-velocity distributions in a transition region between free fall and fluid. The line is a power-law fit $P\sim 1/v^\beta$ with $\beta=7.3$ on the left and $\beta=2.4$ on the right.

Similar velocity distributions (with the same $\alpha=3/2$) have been measured in experiments of *driven* granular systems [14,15]. Such a distribution has also been shown to be a solution to the Boltzmann equation for a system of heated (i.e., with stochastic noise) granular fluid by Noije and Ernst [5] and as a special case of more general multiplicative driving [37]. In our case, the driving is not stochastic (the grains are converting gravitational potential energy into kinetic energy deterministically). However, in the fluid phase the dynamics are apparently sufficiently chaotic to mimic the stochastic noise used in [5,37]. In the free-fall region the direction of particles is predominantly downward with gravity whereas in the fluid region there are more sideways particle collisions which couple the velocity fluctuations in all directions (the anisotropy seen in Fig. 6 disappears). Thus the net result (i.e., the form of the distribution) has the same velocity distribution (with the same $\alpha=3/2$) in the fluid region as is seen in simulations with stochastic noise. It would appear that the stochastic nature is actually essential as the velocity distributions do *not* have this shape in the free-fall

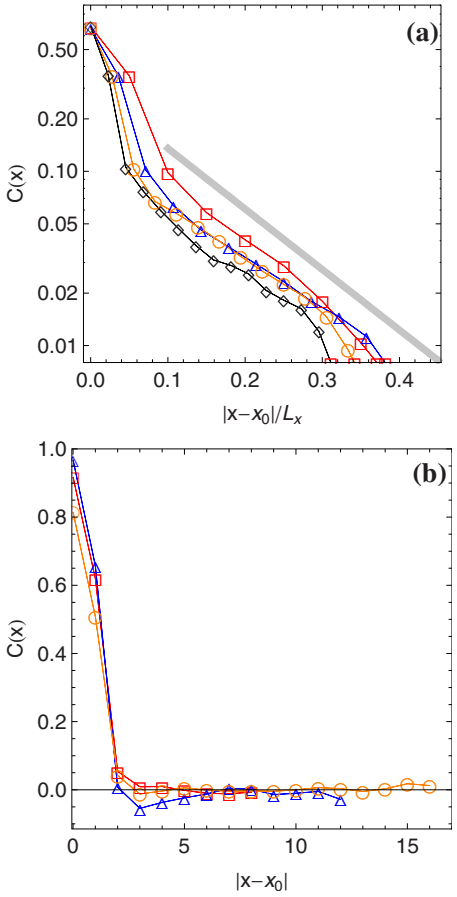

FIG. 10. (Color online) Correlation function $C(x)$ for the x component of the velocity measured from $x_0=L_x/2$ (center of the chute). The sizes of all the systems are $L_x\times 32a\times 400a$, where L_x is the width of the system in the x direction ($L_x=20a$ for the boxes, $28a$ for the triangles, $36a$ for the circles, and $44a$ for the diamonds). (a) Semilogarithmic plot of $C(x)$ for the x component of velocity in the glassy region as a function of the scaled variable $(x-x_0)/L_x$. Data shown in plot (a) is averaged in height in the uniform glassy region at $y_0=90a\pm 20a$. The gray line has a slope of -8, which translates to a length scale $\xi\approx 0.125L_x$ in the relation $\exp\{-(x-x_0)/\xi\}$. (b) $C(x)$ in the fluid region as a function of $|x-x_0|$. The data shown in plot (b) is at a height in the fluid region of the three systems all at the same granular temperature.

regions, where the grain trajectories are too independent to induce chaos, or the glassy region, where the motion of the grains is too coherent.

In the glassy phase, the v_x distribution again fits a Gaussian at low v_x but has exponential tails. In this case, the tails, that are best fit by a function $A\exp(-|v_x/v_0|)$, are closest to filling the distribution near the top of the glassy region and then settle to a fixed fraction of the distribution in bulk of the glassy region. Such distributions have also been seen in experiments of vibrated monolayers of spheres [38,39]. Exponential tails have also been seen in several simulations of dense clusters in two dimensions [37,40]. Such exponential tails have also been derived in the context of driven inelastic Maxwell models with diffusion [4,6,7,41].

We found that our $v_y-\langle v_y\rangle$ distributions in the free-fall and glassy regions showed similar behavior to the v_x distributions described above and as shown in Figs. 7(a) and 7(c). In the fluid region, however, the v_y distribution was dramatically asymmetric about the mean. This distribution can be fit separately on the left and on the right of its peak to functions $A\exp(-(|v_x/v_0|^\alpha)$, with $\alpha=3/2$, as shown in Fig. 7(b). Interestingly, this asymmetry in the v_y distribution has also been found in vibratory experiments [15]. A possible origin of this anisotropy may be that particles going faster than the average downward velocity are more likely to collide than particles going slower than the average.

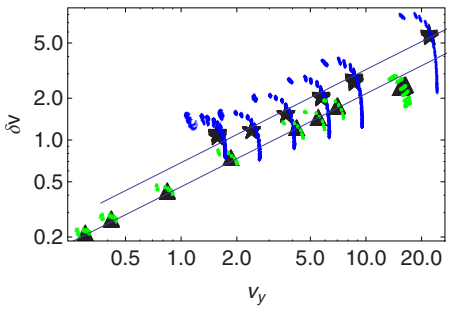

FIG. 11. (Color online) Relationship between fluctuating and flow velocity in the glassy region. Data was averaged in directions normal to $\tilde{\mathbf{g}}$ for the 32×32 [⋆, $\delta v=(\delta v_x^2+\delta v_y^2+\delta v_z^2)^{1/2}$] and 16×16 (▲, $\delta v=\delta v_y$) 15% polydisperse systems. The fitted lines have a slope of $2/3$, in agreement with the experiments of [13]. The points arcing across the line are nonaveraged values of velocities and velocity fluctuations at specific local points in the system.

Clearly, the velocity distribution for each state has very distinct characteristics. As a result, there are transition areas where the velocity distribution changes from one type to another. These crossover areas can give the impression of there being power-law tails in the velocity distributions. Such distributions have also been suggested theoretically as "borderline" cases [6,7]. As an example we examine the transition area between the free-fall and the fluid regions. The velocity distribution for the fluid is wider than that in the free-fall region (cf. Fig. 6) and grows into the free-fall distribution from the tails. The v_x velocity distribution and v_y velocity distribution at roughly halfway through this transition area are shown for one case in Figs. 9(a) and 9(b), respectively. As can be seen, the tails of these distributions can be fit to $P\sim 1/v^\beta$ with $\beta=3.8$ for both tails of the v_x distribution and with $\beta=7.3$ and $\beta=2.4$ for the left and right tails of the v_y distribution rather convincingly. Theory [6–8] suggests considerably higher exponents for the power laws. Interestingly, our exponents are very close to the experimentally determined power-law exponents of $\beta=3.6$ for the tails of the v_x distribution and $\beta=7.4$ and $\beta=2.9$ for the tails of the v_y distribution found recently in an experiment by Moka and Nott [16]. Their experiment configuration is very similar to our simulation and the characteristics of the average velocity profile and the profile of velocity fluctuations are consistent with what we find in the free-fall to fluid transition area (compare Fig. 1 of [16] with the appropriate profiles in our Figs. 3 and 5). It is not clear that this is a true power law as it corresponds to a crossover area and while we have just over three decades in height, we do not have a full decade in width. However, it is possible that the equivalent area in the

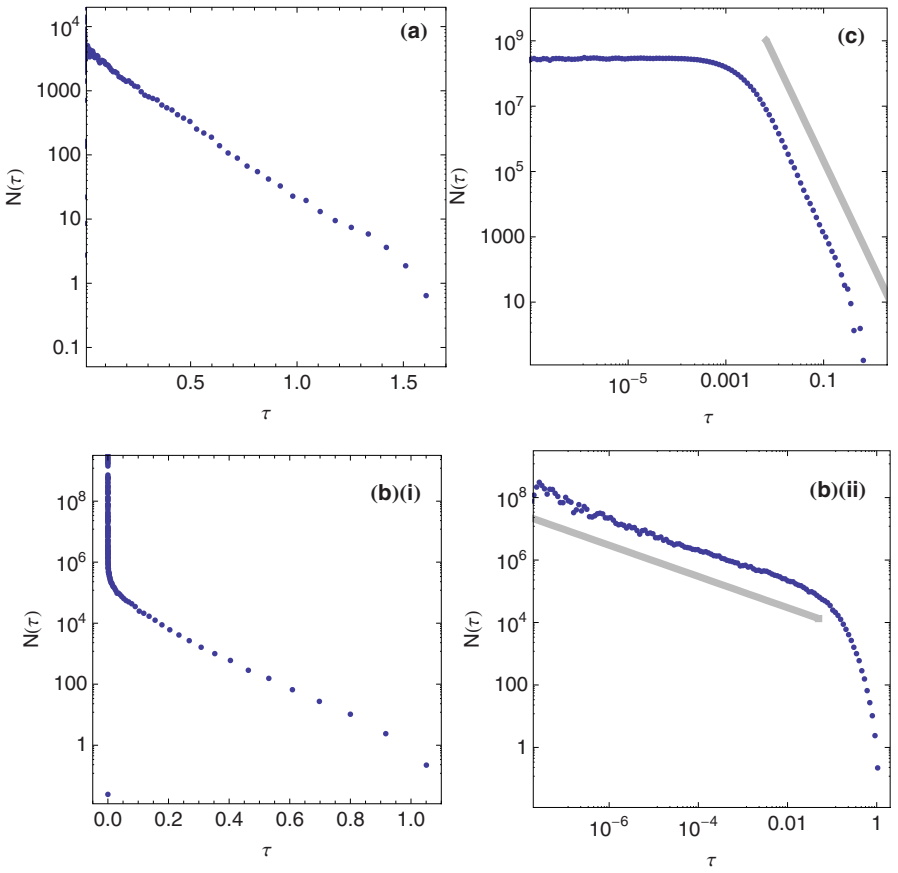

FIG. 12. (Color online) In a 15% polydisperse 3D $32\times32\times250$ simulation with a probability of reflection p of 10% at the bottom of the chute, (a) semilogarithmic plot of collision time distribution at the top of a fluid region at $h=190$, (b)(i) semilogarithmic plot on the left, and (b)(ii) log-log plot on the right of the collision time distribution in a fluid-glass transition region at $h=165$ (the sloped straight line in the log-log plot on the right has a slope of −0.5), and (c) log-log plot of collision time distribution in a glassy region at $h=90$ (the sloped straight line has a slope of −3).

experiment is wider than we see in our simulations due to some aspect that we are not including (such as particle spin). It would be interesting to see the experiment results at a range of heights along the column as we have done here in the simulations.

V. VELOCITY CORRELATIONS

As the particles undergo collisions traveling down the chute, they lose some of their relative velocity v_n, and hence become more correlated. In order to compare how the particles become correlated within the chute, we measured their v_x velocity-velocity correlation function every $5a$ from the top to bottom of the chute. In particular, we compared the velocity correlations of the particles in the glassy and fluid regions and found a noticeable difference in the way the velocity correlations scale.

We ran simulations with different sized system widths L_x, in the x direction, while keeping the dimensions in the y direction and z direction the same. Note that as the walls are at $x=0$ and $x=L_x$, $\langle v_x\rangle=0$. Based on our data for system widths of $20a$, $28a$, $36a$, and $44a$, the $\langle v_x(x_0)v_x(x)\rangle$ velocity correlations,

$$C(x)=\frac{\langle v_x(x)v_x(x_0)\rangle}{[\langle v_x^2(x)v_x^2(x_0)\rangle]^{1/2}}, \tag{4}$$

for various system sizes are shown in Fig. 10. The form of the tails of the velocity correlations in the glassy region follow an exponential decay, $\exp\{-(x-x_0)/\xi\}$. This is demonstrated by the straight portions of the curves in the semilogarithmic plot shown in Fig. 10(a). Remarkably ξ scales only with system size, $\xi=0.125L_x$. [The lines in Fig. 10(a) are parallel and the x axis is already scaled by L_x.] The slope of the gray line in Fig. 10(a) corresponds to $\xi=0.125L_x$.

We also tried looking at 2D correlation functions $\langle v_x(y_0)v_x(y)\rangle$. The correlation length was similar in the y direction, although the data for the 2D correlation function was much noisier [as it was measured relative to a single point (x_0,y_0,z_0) and so could not benefit by the averaging over different y_0 that was done for the 1D correlation functions]. As the weight of the glassy column is supported by the walls, essentially through what is expected to be an arching effect [28], the similarity of correlation lengths in the x and y directions is expected.

Interestingly, in the fluid region, the $\langle v_x(x_0)v_x(x)\rangle$ velocity correlations drop to zero at a length of around $3-5a$, where a is the mean particle radius. This is shown in Fig. 10(b), which plots the velocity correlations in the fluid region for three different sized systems, but at the same granular temperature. Thus we can clearly see that how the correlations scale also distinguishes between a glassy and fluid phase in granular matter. It would be interesting if experiments could measure velocity correlations in different phases of granular matter to compare with our findings.

VI. PROPERTIES RELATED TO VELOCITY FLUCTUATIONS

Previous work has suggested a possible relationship between the velocity fluctuations, $\delta v\equiv|\delta\mathbf{v}^2|^{1/2}$, and the flow

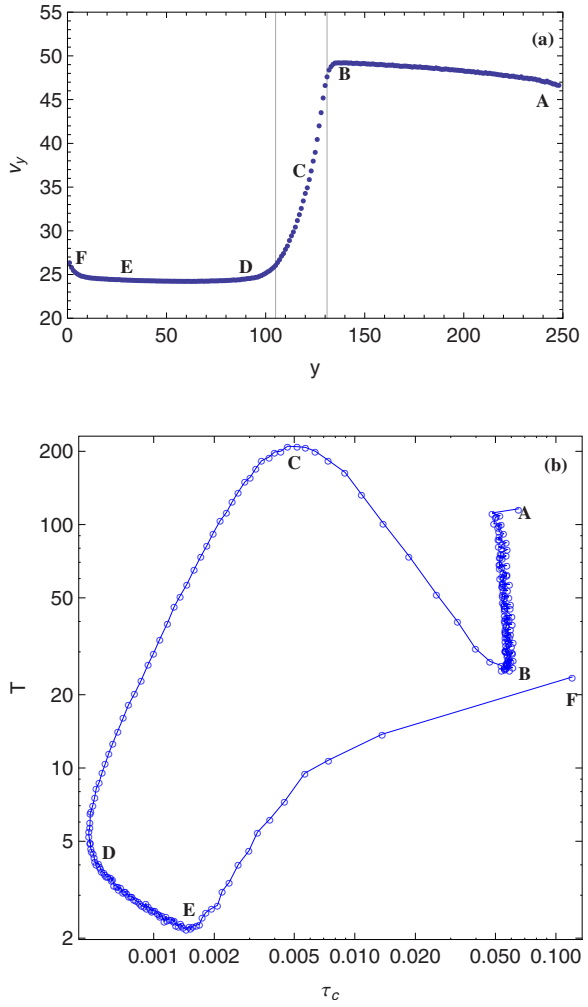

FIG. 13. (Color online) Mapping of points A, B, C, D, E, and F between (a) v_y velocity profile along chute height y and (b) log-log plot of velocity fluctuations as measured by the granular temperature T, versus mean collision time τ_c in a 15% 3D $32\times32\times250$ simulation with $p=0.01$. The free-fall region runs between points A and B. The free-fall to fluid transition region runs between points B and C. The fluid region runs between points C and D. The glassy region runs between points D and E. Between points E and F the material becomes fluid again near the bottom sieve. Here, p is the probability of reflection at the bottom of the chute and the asymptotic coefficient of restitution $\mu_0=0.9$.

velocity $\mathbf{v}$. In [19] we used our simulations to confirm Menon and Durian's diffusing wave spectroscopy experiment [13] that showed the fluctuating velocity is power-law related to the flow speed v_y of particles falling under the influence of gravity in a vertical chute, $\delta v \propto v^{2/3}$ (Fig. 11). An important detail is that we arrived at this 2/3 power law only after we had averaged our data across the x direction of the chute (in the glassy region). This is similar to the experiment, where diffusing wave spectroscopy was used. Such an experiment involves looking at the correlation of laser speckle patterns after the laser beam has traversed the width of the chute. Note, however, from Fig. 5(c) that the velocity fluctuations are not constant across the channel. Plotting δv locally (i.e., the profile across the chute rather than the average), we get the curved branches in Fig. 11. Note that the actual profiles cross the average perpendicular to our 2/3 power-law line. Thus this power law is a nonlocal, averaged effect.

In our previous paper [19] we studied collision time distributions in the glassy and fluid regions. Here we will examine how the collision time distribution changes from one region to the other and how the collision times are related to the velocity fluctuations. The average collision time (the time between successive collisions for a particle) is

$$\tau_c \equiv \langle \tau \rangle = \frac{\int_{t_s}^{t_b} \tau N(\tau) d\tau}{\int_{t_s}^{t_b} N(\tau) d\tau}, \tag{5}$$

where $N(\tau)$ is the histogram of collision times observed in one of our simulations, and t_s and t_b are upper and lower cutoffs. Figure 12 shows the collision distributions for different regions of our simulations. For the analytic form of the collision time distributions that we will compare our simulation data to,

$$\langle \tau \rangle = \begin{cases} t_m & \text{for } N(\tau) \sim e^{-\tau/t_m} \\ 2t_s & \text{for } N(\tau) \sim \tau^{-3}, \quad t_b \to \infty, \\ \dfrac{1}{3} t_b & \text{for } N(\tau) \sim \tau^{-1/2}, \quad t_s \to 0. \end{cases} \tag{6}$$

Thus, the mean collision time tends to zero, or the lower cutoff, for the τ^{-3} case whereas it tends to the upper cutoff for the $\tau^{-1/2}$ case.

As can be seen from Fig. 12, in the fluid region we have an exponential distribution of collision times and therefore a well-defined mean collision time $\langle \tau \rangle$, t_m from Eq. (6). As shown in Fig. 12(a), in the glass, $N(\tau) \sim \tau^{-3}$ as reported in our recent paper [19]. This is shown in Fig. 12(c) for one of the faster systems. In the glass, $\langle \tau \rangle$ is essentially equal to the lower cutoff of the power law [see Eq. (6)]. In the fluid-glass transition region $N(\tau) \sim \tau^{-1/2}$ as shown in Fig. 12(b). In this case $\langle \tau \rangle$ is at the upper cutoff, Eq. (6), corresponding to the crossover to the exponential tail. The $\tau^{-1/2}$ power law exists only over a narrow band of heights and disappears by the exponential tail continuously turning into the τ^{-3} glass distribution. The crossover between the resulting two power laws (t_b for $\tau^{-1/2}$ and t_s for τ^{-3}) moves lower as one goes into the glass. The existence of the $\tau^{-1/2}$ power law is somewhat curious as it does not correspond to either the fluid or glassy states. However, the way it disappears as we go into the glass provides a clue. If one associates the glass with a "collapsing condensate" [1,2,4], the fluid to glass transition should involve "droplets" of collapsing condensate coming out of the fluid. In each droplet, the collision times should be distributed as in the glass, but the cutoff t_s will depend on how close the droplet is to the close-packed glass density. Droplets of different sizes are then likely to have different cutoffs. A wide distribution of droplet sizes will then result in a wide distribution of cutoffs for the $N(\tau) \sim \tau^{-3}$ power law, perhaps generating the $\tau^{-1/2}$ low end tail seen in the transition regime.

We now examine the relationship between the velocity fluctuations, as measured by the granular temperature $T = (\langle v_x^2 \rangle + \langle v_y - \langle v_y \rangle^2 \rangle + \langle v_z^2 \rangle)/2$ and the collision times. Figure

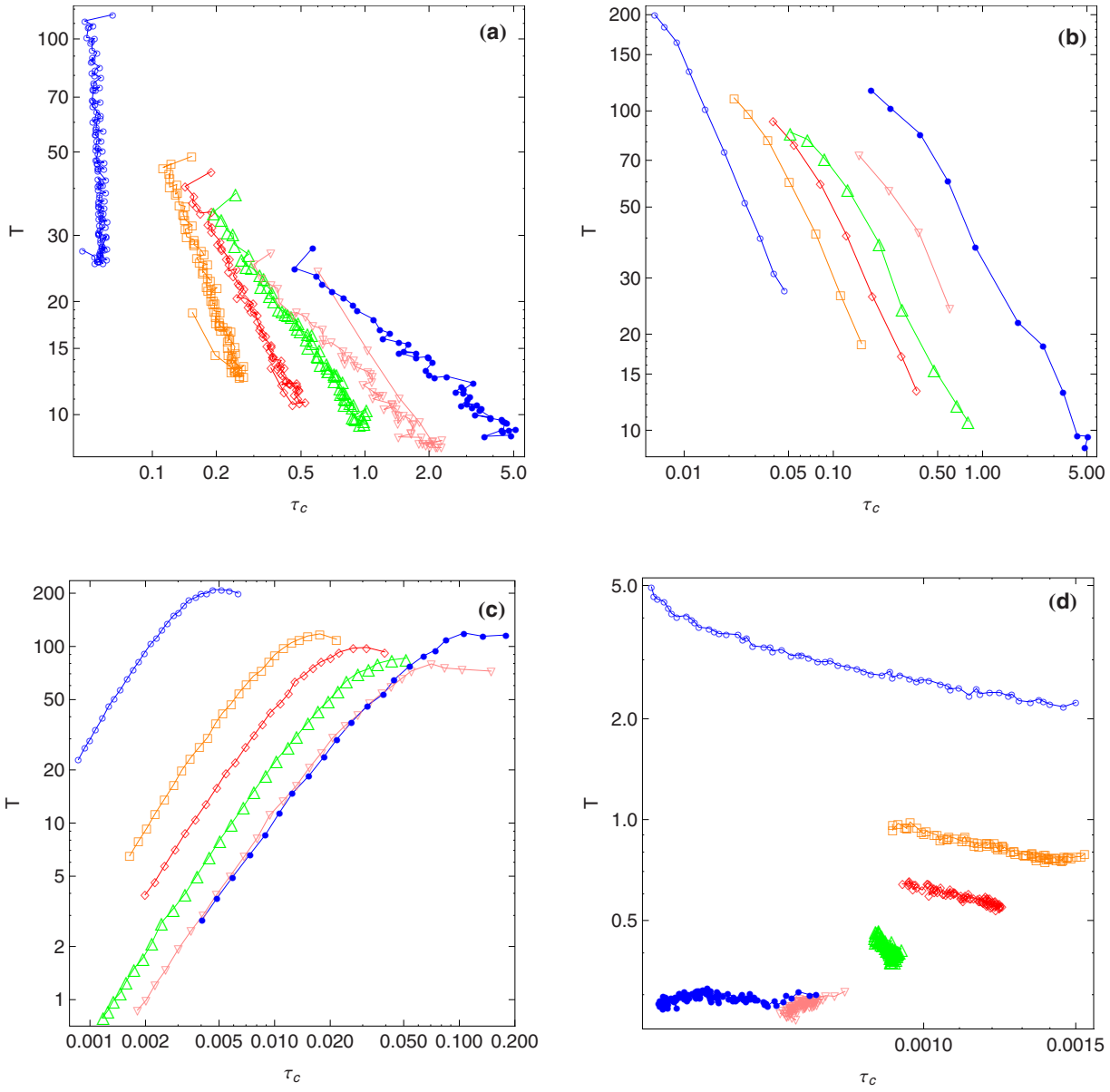

FIG. 14. (Color online) Log-log plot of velocity fluctuations as measured by the granular temperature T, versus mean collision time τ_c in (a) free-fall region, (b) free-fall to fluid transition, (c) fluid region and (d) glassy region in a 15% 3D $32\times32\times250$ simulation with (○ with $p=0.01$), (□ with $p=0.1$), (◇ with $p=0.25$), (△ with $p=0.5$), (▽ with $p=0.75$), and (● with $p=0.9$). Here, p is the probability of reflection at the bottom of the chute and the asymptotic coefficient of restitution $\mu_0=0.9$.

13(a) shows the velocity profile for a very fast flowing system (with probability of reflection at the bottom of the chute of $p=0.01$). The transitions between different phases are marked by capital letters. We can map these labeled points that mark the boundaries between the different regions onto a plot of T vs τ_c shown in Fig. 13(b). The different regions show *very* different relationships between T and τ_c. To see if these relationships are general, or system specific we look at several systems with different probabilities of reflection at the bottom of the chute, and hence very different flow rates. By plotting the different systems on the same log-log plot, as shown in Fig. 14, we can observe whether there is a power-law relationship between T and τ_c in each of the different regions. As can be seen from the figure there exists a power-law relationship $T=\tau_c^{\gamma}$ in the free-fall or fluid transition with γ around -1.1 (the lines are all parallel and have slope -1.1) and in the fluid region with γ around 1.4, but there is no obvious relationship in the free-fall and glassy regions.

In Fig. 15 we examine the fluid and glass regions corresponding to different values for the probability of reflection at the bottom of the chute, p [42]. As shown in Fig. 15, the faster systems with lower reflection probabilities of p such as 10% tend to *turn around* at the fluid to glass transition and reach a limiting line. The slower systems with higher reflection probabilities such as 75% both fall on the same limiting line. This behavior can be explained as follows. The simulation with $p=10\%$ is a much faster flow so its y velocity, density, and velocity fluctuations are not a constant value in the "glass." For example, the density at the top of the glassy region for the fast flows is slightly lower and gradually in-

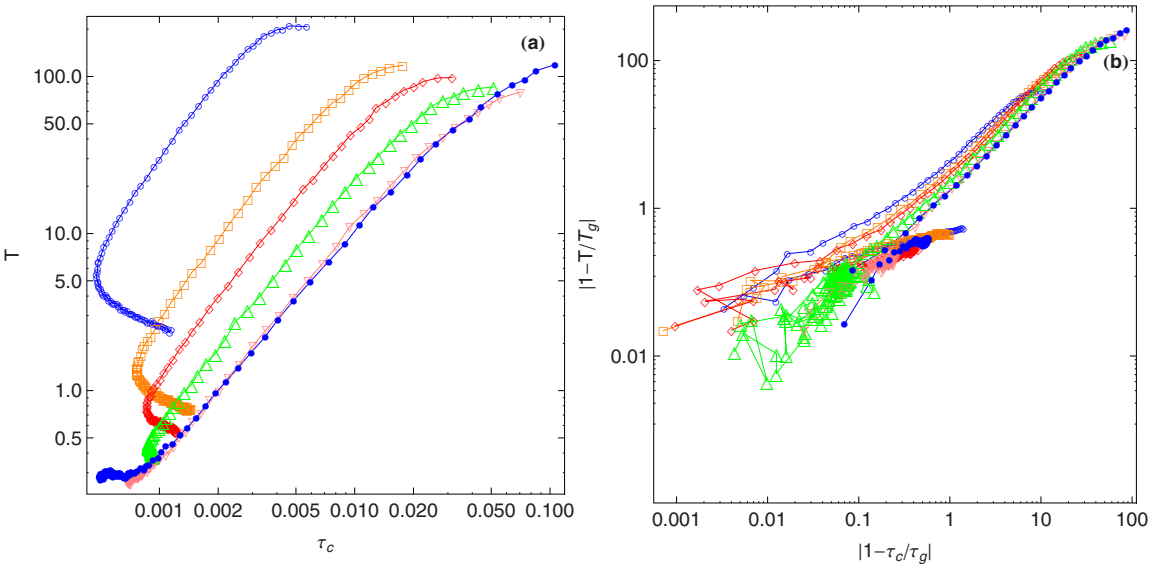

FIG. 15. (Color online) (a) Granular temperature T versus mean collision time τ_c, and (b) temperature versus mean collision time scaled by the glass transition temperature, T_g and the corresponding collision time τ_g in a 15% 3D $32\times32\times250$ simulation with (○ with $p=0.01$), (□ with $p=0.1$), (◇ with $p=0.25$), (△ with $p=0.5$), (▽ with $p=0.75$), and (● with $p=0.9$). Here, p is the probability of reflection at the bottom of the chute and the asymptotic coefficient of restitution $\mu_0=0.9$.

creases as one goes further into the glass. Thus the system is unable to reach a stationary, or in other words translationally invariant, steady state.

It is also worthwhile to consider the fluid to glass transition regions in terms of the jamming phase diagram proposed by [43]. They propose a "jammed" phase diagram as a function of temperature, density, and shear stress where the region in the vicinity of the origin is jammed and the region far from the origin is not jammed. Their jamming transition is expected to be first order except for the J point, a transition at close packing density and at $T=0$ and where the shear stress is zero. The transitions for the different systems seen in Fig. 15 occur at different temperatures and different shear stresses (related to the flow speed controlled by the probability of reflection p). As we lower the flow speed, and the temperature at which the transition occurs decreases, our system should be approaching the J point, and the transition should become more continuous and the "glass" state should approach a more well-defined translationally invariant, disordered limit. This is consistent with what we observe in Fig. 15. If we attempt to scale Fig. 15(a) by the difference in temperature from the observed transition for each system, we arrive at Fig. 15(b). We find that the slower systems start to approach a single universal line but the faster systems deviate. While a full investigation of the transition is beyond the scope of the current paper, we plan to investigate this more in the future.

VII. CONCLUSIONS

In this paper we have examined velocity fluctuations in computer simulations of a granular system. The gravity-driven granular chute flow system we study has been realized in numerous experiments. Our observations are consistent with the fluctuations observed in the experiments most closely matching our simulations [13,16].

We find three main classes of velocity distributions corresponding to the free-fall, fluid, and glassy regions. In the free-fall region we see a Gaussian distribution of velocities, but the velocity fluctuations in the vertical and horizontal direction evolve separately. In the fluid region the velocity distribution has a stretched exponential tail of $\exp(-v^{3/2})$, but the vertical velocity fluctuations become very asymmetric and require separate fits for velocities above and below the mean. In the glassy state the velocity distribution has exponential tails. Velocity fluctuations are correlated on the scale of the system size in the glassy region and have a finite correlation length independent of system size in the fluid region.

We then related the velocity fluctuations to the collision time, the time between collisions. The distribution of collision times in the glass is power-law distributed and in the fluid it is exponential, as we observed in previous work [19]. We also find evidence that the transition from fluid to glass becomes more continuous for slower-moving, lower temperature flows. The slower flows also reach a more translationally invariant disordered glassy state. These observations are consistent with the approach to the J point defined by O'Hern and collaborators [43].

ACKNOWLEDGMENTS

This work was supported by the Natural Science and Engineering Research Council of Canada, the Ontario Graduate Scholarship Program, and SharcNet.

[1] I. Goldhirsch and G. Zanetti, Phys. Rev. Lett. **70**, 1619 (1993).
[2] S. McNamara and W. R. Young, Phys. Rev. E **50**, R28 (1994).
[3] I. S. Aranson and L. S. Tsimring, Rev. Mod. Phys. **78**, 641 (2006).
[4] S. Esipov and T. Poschel, J. Stat. Phys. **86**, 1385 (1997).
[5] T. P. C. van Noije, M. H. Ernst, R. Brito, and J. A. G. Orza, Phys. Rev. Lett. **79**, 411 (1997).
[6] M. H. Ernst and R. Brito, Phys. Rev. E **65**, 040301 (2002).
[7] M. H. Ernst and R. Brito, J. Stat. Phys. **109**, 407 (2002b).
[8] E. Ben-Naim and J. Machta, Phys. Rev. Lett. **94**, 138001 (2005).
[9] V. V. R. Natarajan, M. L. Hunt, and E. D. Taylor, J. Fluid Mech. **304**, 1 (1995).
[10] R. M. Nedderman and C. Laohakul, Powder Technol. **25**, 91 (1980).
[11] H. Takahashi and H. Yanai, Powder Technol. **7**, 205 (1973).
[12] S. B. Savage, J. Fluid Mech. **92**, 53 (1979).
[13] N. Menon and D. J. Durian, Science **275**, 1920 (1997).
[14] W. Losert, D. G. W. Cooper, J. Delour, A. Kudrolli, and J. P. Gollub, Chaos **9**, 682 (1999).
[15] F. Rouyer and N. Menon, Phys. Rev. Lett. **85**, 3676 (2000).
[16] S. Moka and P. R. Nott, Phys. Rev. Lett. **95**, 068003 (2005).
[17] W. Losert, L. Bocquet, T. C. Lubensky, and J. P. Gollub, Phys. Rev. Lett. **85**, 1428 (2000).
[18] L. Bocquet, W. Losert, D. Schalk, T. C. Lubensky, and J. P. Gollub, Phys. Rev. E **65**, 011307 (2001).
[19] J. J. Drozd and C. Denniston, Europhys. Lett. **76**, 360 (2006).
[20] We use units where the acceleration due to gravity $g=1$, the mean grain radius $a=1$, and the mean grain mass $m=1$. To convert to units where, say, $g=9.8\ \mathrm{m/s^2}$, $a=1.5\ \mathrm{mm}=1.5\times10^{-3}$ m, and $m=0.11\ \mathrm{g}=1.1\times10^{-3}$ kg (i.e., a steel ball with mass density of $7850\ \mathrm{kg/m^3}$), multiply our distance by a in meters, time by $(a/g)^{1/2}=[(1.5\times10^{-3}\ \mathrm{m})/(9.8\ \mathrm{m/s^2})]^{1/2}=0.0124$ s and masses by m in kilograms. A typical simulation run is 10^4–10^5 time units, or 2–20 min of real time for a system made up of steel balls 3 mm in diameter. For a typical run with polydisperse grains, this corresponds to 6.5×10^9 collisions.
[21] C. Denniston and H. Li, Phys. Rev. E **59**, 3289 (1999).
[22] J. T. Jenkins and S. B. Savage, J. Fluid Mech. **130**, 187 (1983).
[23] S. B. Savage and D. J. Jeffrey, J. Fluid Mech. **110**, 255 (1981).
[24] C. Bizon, M. D. Shattuck, J. B. Swift, W. D. McCormick, and H. L. Swinney, Phys. Rev. Lett. **80**, 57 (1998).
[25] S. Luding, E. Clement, J. Rajchenbach, and J. Duran, Europhys. Lett. **36**, 247 (1996).
[26] W. Goldsmith, *Impact: The Theory and Physical Behaviour of Colliding Solids* (E. Arnold, London, 1960), pp. 263–267.
[27] Typical fluctuation velocities are $\delta v=0.05$ implying $\mu\approx0.99$.
[28] K. To, P. Y. Lai, and H. K. Pak, Phys. Rev. Lett. **86**, 71 (2001).
[29] J. Duran, *Sands, Powders, and Grains: An Introduction to the Physics of Granular Materials*, Partially Ordered Systems (Springer, New York, 2000), ISBN 0387986561.
[30] L. D. Landau and E. M. Lifshitz, *Fluid Mechanics*, Course of Theoretical Physics Vol. 6, 2nd ed. (Pergamon Press, Oxford, England; Toronto, 1987), ISBN 0080339336.
[31] H. Reiss and A. D. Hammerich, J. Phys. Chem. **90**, 6252 (1986).
[32] E. Khain, Phys. Rev. E **75**, 051310 (2007).
[33] E. Khain, B. Meerson, and P. V. Sasorov, Phys. Rev. E **70**, 051310 (2004).
[34] R. Liu, Y. Li, M. Hou, and B. Meerson, Phys. Rev. E **75**, 061304 (2007).
[35] M. Schröter, S. Nägle, C. Radin, and H. L. Swinney, Europhys. Lett. **78**, 44004 (2007).
[36] J. S. van Zon and F. C. MacKintosh, Phys. Rev. Lett. **93**, 038001 (2004).
[37] R. Cafiero, S. Luding, and H. J. Herrmann, Phys. Rev. Lett. **84**, 6014 (2000).
[38] J. S. Olafsen and J. S. Urbach, Phys. Rev. Lett. **81**, 4369 (1998).
[39] J. S. Olafsen and J. S. Urbach, Phys. Rev. E **60**, R2468 (1999).
[40] H. J. Herrmann, S. Luding, and R. Cafiero, Physica A **295**, 93 (2001).
[41] A. V. Bobylev and C. Cercignani, J. Stat. Phys. **106**, 547 (2002).
[42] In our recent paper on collision time distributions [19], our reflection probability p value was incorrectly stated to be 10%. It was actually a p value of 90%, or in other words, our collision times were measured for a very slow flow of particles.
[43] C. S. O'Hern, L. E. Silbert, A. J. Liu, and S. R. Nagel, Phys. Rev. E **68**, 011306 (2003).